Probabilistic multi-objective optimization of wood torrefaction conditions using a validated mechanistic model

Daniela Florez, Antoine Stéphan, Patrick Perré, Romain Rémond

Probabilistic multi-objective optimization of wood torrefaction conditions using a validated mechanistic model

Daniela Florez[a,*], Antoine Stéphan[a], Partrick Perré[b,c], Romain Rémond[a]

[a]LERMAB, Laboratoire d'Etude et de Recherche sur le Matériau Bois, EA 4370 USC 1445 INRA, ENSTIB. Université de Lorraine, 27 rue Philippe Séguin, 88000, Epinal, France [email: daniela-carolina.florez-parra@univ-lorraine.fr; antoine.stephan@univ-lorraine.fr; romain.remond@univ-lorraine.fr]

[b]LGPM, Centrale Supélec, Centre Européen de Biotechnologie et de Bioéconomie (CEBB), Université Paris-Saclay, 3 rue des Rouges Terres, 51110, Pomacle, France

[c]LGPM, CentraleSupélec, Université Paris-Saclay, 8-10 rue Joliot-Curie, 91190, Gif-sur-Yvette, France [email : patrick.perre@centralesupelec.fr]

*Corresponding author.

Abstract

This paper uses a comprehensive computational model to propose optimal wood torrefaction conditions by probabilistic optimization. Its main outcome is to propose tailor-made heat treatment conditions (temperature levels-duration of mild pyrolysis at temperature levels ranging from 200 to 300 °C) to meet users' expectations in terms of overall mass loss, duration and homogeneity of treatment. To this purpose, beech wood boards were torrefied with a usual 3-steps treatment schedule (drying, heating and cooling) under contrasting configurations in a well-instrumented device. The heterogeneity of the treatment within the wood sample was assessed through X-ray attenuation profile and water vapour sorption isotherm. These results allowed the model to be validated. In particular, it predicts the evolution of the mass loss and internal temperatures with good accuracy, including the temperature overshot. The results highlight the need to adjust the heat treatment schedule to each input parameter such as the wood piece dimensions and its initial moisture content or density, in order to limit the effect of exothermic reactions. The torrefaction model was then embedded in a probabilistic optimization process. A case

study demonstrates the ability of the model to propose an alternative 3-steps treatment schedule able to reach the target mass loss while controlling the temperature overshot within the wood piece.

Keywords: Wood torrefaction, thermal modification, optimal conditions, treatment heterogeneity, overheating, computational model.

1. Introduction

Torrefaction of wood is a mild pyrolysis treatment at temperature levels ranging from 200 to 300 °C in the absence of oxygen. This induces the thermal alteration of the cell wall constituents of wood, namely hemicelluloses, cellulose and lignin, via a series of thermally activated chemical reactions coupled with heat and mass transfer phenomena. Chemical modification concerns mainly hemicelluloses degradation, lignins reticulation and modification of the crystalline structure of the cellulose [1–7].

Over the last 50 years, torrefaction has been used to effectively improve various wood properties such as durability and dimensional stability [8–10]. These studies were intended for solid wood as a material. Later, torrefaction was promoted for other purposes. Current perspectives of this technology aim at taking advantage of renewable resources, to valorize wood and biomass wastes, thus limiting the exploitation of natural resources. For example, in an attempt to replace fossil fuels, a pre-treatment by torrefaction of woody biomass is advised to obtain hydrophobic products with increased specific energy contents and improved grindability [11–14]. Besides, it also leads to increased anti-shrinkage efficiency, which reduces swelling during moisture recovery, which is an interesting feature for wood chips stored in a silo. Furthermore, torrefaction can be advantageous in processing heterogeneous cellulosic feedstock of different density, humidity content and size, such as those from forestry (logs, chips, sawdust, bark, etc.) or agricultural crops [15,16]. These characteristics make torrefaction suitable for integration into existing commercial regimes such as the white wood pellet value chain [15,17]. Moreover, end-of-life wooden furniture may be recycled and decontaminated by removing the urea-formaldehyde and melamine-formaldehyde resins through a low temperature pyrolysis [18,19]. This opens the possibility to use recycled wooden furniture materials for energy production. Nonetheless, the introduction of the torrefaction technology in industrial manufacturing processes can pose serious safety issues with regards to fire and injury risks. In this respect, various authors have reported that overheating

occurs within wood products induced by the exothermic reactions during torrefaction. Indeed, as wood has a low thermal conductivity, the internal source of heat due to exothermic reactions gives rise to an important temperature gradient needed to drive heat towards the exchange surfaces. The core temperature therefore increases with, and in turn, activates even more, the exothermic reactions [20–22]. A thermal runaway is then likely to occur at the scale of a boards stack or a packed bed of wood chips where a dual-scale interaction occurs. The wood piece supplies the energy to the airflow due to the exothermic reactions, the gas temperature increases along the stack or the packed bed which triggers even more the exothermic reactions along the flow direction [23]. The risk of thermal runaway depends on the size of the wood piece and process conditions (heating rate, airflow velocity, temperature, etc.). In addition to safety issues, this produces also a heterogeneous treatment, both within and between the wood pieces, hence undesirable consequences on the mass yield and product quality. Nowadays, however, torrefaction programs are often empirical and customized according to the wood species (softwood, hardwood, density, etc.), the characteristics of the products to be torrefied (e.g., dimensions, geometry, initial moisture content, etc.) and the user expectations.

The motivation for this research arises from the difficulty of determining the optimal torrefaction schedule that could limit the overheating within the wood piece and ensure that products meet quality requirements, for example the hydrophobic character, energy content and grindability for energy purposes, or the anti-shrinkage efficiency, mechanical performance and color for solid wood. Since most of these properties are monotonic functions of the overall mass loss [11,24–28], the latter could therefore be used as a target indicator to fine-tune the torrefaction parameters (duration–temperature levels) in order to meet quality specifications.

In the present work, the research approach consists of two complementary parts. In the first, in a series of experiments, beech (*Fagus sylvatica*) wood boards were torrefied using the usual 3-step program (drying, heating at high temperature and cooling) under different conditions in terms of the sample thickness and initial moisture content. The experimental data, including local values of internal sample temperatures and mass loss progression, were then compared with simulations of a torrefaction model [22,29–31]. The comparison between simulation and measurement in contrasting configurations

allowed the robustness of the model to be assessed. In the second part, this model was integrated into an optimization algorithm with the purpose of proposing optimized heat treatment schedules (temperature levels and durations), meeting the user expectations in terms of mass loss, duration and homogeneity of treatment, while mitigating the undesirable overheating within the wood piece. A case study was conducted to experimentally validate one of the treatment schedules proposed by the optimization procedure.

2. Measuring the torrefaction kinetics and treatment homogeneity under contrasting conditions

2.1 Materials

In order to focus on the effects of different factors such as the sample thickness and initial moisture content on the homogeneity of the heat treatment, the sampling was designed to limit the effect of the biological variability of wood (Fig. 1a). For that purpose, a green beech (*Fagus sylvatica*) log from the Vosges region in France, with a diameter of about 60 cm, was selected and sawn. Then, two flatsawn boards were selected at least 10 cm far from the bark to keep only the heartwood, and each board was cut into specimens of final dimensions 20 mm (R) x 150 mm (T) x 300 mm (L) and 40 mm (R) x 150 mm (T) x 280 mm (L). Note that the large volume/surface ratio of the solid wood samples used here are more demanding as they exacerbate the intra-particle temperature peak due to the importance of internal transfers. Such sizes also ensure the reliability and accuracy of the experimental measurements (mass evolution and internal temperature). Smaller volume/surface ratios encountered in energy applications could be easily predicted by this mechanistic model as these situations limit the coupling due to internal transfers. The boards were pre-conditioned at 12 % of moisture content on dry basis (MC) in a climatic chamber at 40 °C and 75 % of relative humidity.

Subsequently, the specimens were instrumented with thermocouples of 1 mm diameter with a gas-tight *Swagelok* connector to link the board to the probe. As illustrated in Figure 2, they were placed half-length and mid-width of the boards, 75 mm deep from the lateral surface (RL plan). One was inserted at the core (half thickness) and the second at about 2 mm from the surface (TL plan). Finally, the

endpieces of the boards were coated with a silicone film maintained by two metallic parts strongly tied (see Fig. 2), to prevent mass transfer in the longitudinal direction and avoid any gas leakage due to overpressure during the treatment. This leads the boards to have a behavior similar to that of long boards with transfers mainly in the radial and tangential directions.

2.2 Methods

2.2.1 Experimental setup

The heat treatment experiments were carried out in an experimental reactor designed for this purpose (Fig. 2), inspired by Colin's thesis work [32]. It consists of an oven Memmert UF110 plus equipped with four polished stainless-steel heating walls (top, bottom, and sides) heated by electric resistances, two temperature probes placed in the middle and top of the oven chamber, and a tangential fan on the back wall. The maximum working temperature is 300 °C (setting accuracy of 0.5 °C) and the heating rate can be precisely tuned in the range of 1 to 10 °C min^{-1}. The fan ensures the circulation of the gases, and its velocity, adjustable in 10 % steps, was set at 40 % for all experiments. The complex air velocity inside the chamber is not known, but, as explained below, the heat transfer coefficient, the pertinent parameter, has been determined experimentally. Below the reactor, a digital balance is placed in a hermetic chamber, which communicates with the reactor chamber through a glass tube (inner diameter of 12 mm) embedded under the reactor bottom wall. Glass is chosen here because of its lower thermal conductivity compared to metal. The wood specimen is attached to a sample holder, placed in the reactor chamber, that stands directly on a tripod resting on the balance, both of which are clamped to the ends of a glass rod (8 mm diameter) passing through the glass tube. The system is continuously swept by a nitrogen flow (5 L min^{-1}) at room temperature and fed into the weighing chamber. To prevent cooling of the reactor chamber by the flow of nitrogen, an aluminum plate (3 mm thick) was placed 3 cm above the bottom wall of the oven, thus creating a preheating chamber that retains and heats the entering gas before letting it flow through the main chamber. The volatile products are exhausted from the side of the reactor. The oxygen level is continuously measured at the outlet flow by using an oxygen analyzer with a zirconium oxide sensor (ZOA 100). The whole system was remotely controlled and monitored

by a home-made software developed on LabView. The oven temperature distribution was measured during torrefaction and only small differences of about 3 °C were recorded between the middle and top of the chamber. The middle temperature was lower than the set point by 2 °C.

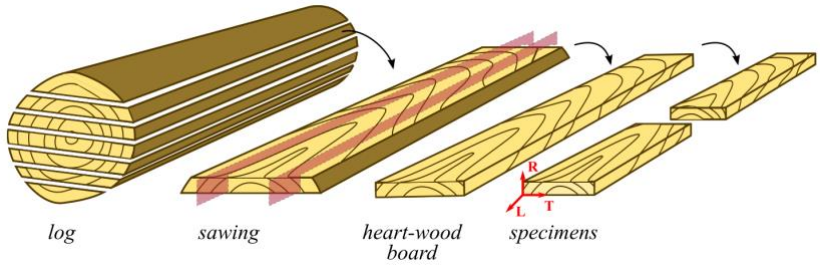

a) Sampling pre-treatment

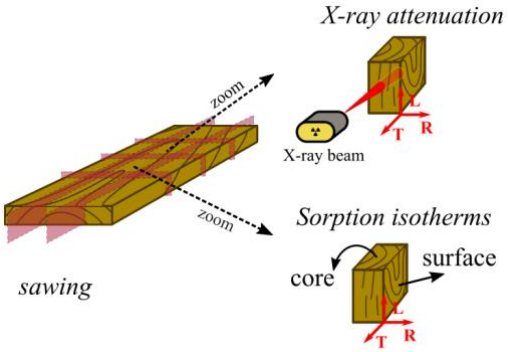

b) Post-treatment of torrefied samples

Fig. 1. Overview of the experimental study: (a) sampling pre-treatment of the wood boards and (b) post-treatment analysis of heat-treated boards.

The overall external heat transfer coefficient of the reactor was determined by considering the contribution of the convective and radiative transfers. On the one hand, the convective heat transfer coefficient was assessed experimentally by the sponge method [33] at a temperature of 50 °C, for which radiation is low, and under flow conditions similar to those used for the torrefaction experiments. A value of about 12 W m^{-2} K^{-1} was determined for this parameter. On the other hand, the contribution of the heat transfer by emitted radiation, from the oven surfaces to the boards, was estimated according to the Stefan–Boltzmann law. The radiative heat transfer at the torrefaction temperature (i.e., 230 °C) was

144 estimated about 13 W m^{-2} K^{-1}. In this work, the overall external heat transfer coefficient of the
145 torrefaction reactor was found to be of the order of 35 W m^{-2} K^{-1}.

146

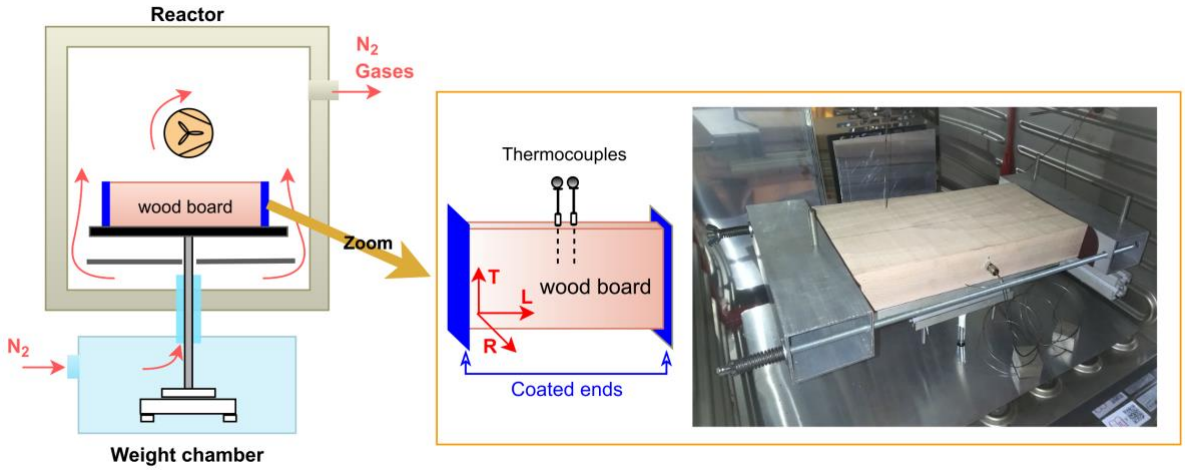

147

148 **Fig. 2**. Reactor device for wood torrefaction treatment and photo of one instrumented board.

149 *2.2.2 Torrefaction conditions*

150 The course of the torrefaction was monitored in real time through the following parameters:
151 temperatures of the reactor chamber (middle and top) and board (core and subsurface), oxygen level at
152 the outlet flow (e.g., less than 2 %) and mass loss. The experimental conditions of the heat treatment
153 (HT) schedules performed on the four single board specimens are detailed in Table 1. The usual 3-phase
154 schedule was applied on these boards: (1) a drying period at 110 °C for at least 1 hour; (2) heating at a
155 rate of 7 °C min^{-1} until the treatment temperature of 230 °C; then maintained at this level for 3 hours;
156 (3) and finally cooled down at a rate of 2 C min^{-1} until the temperature decreases to 150 °C in the reactor.
157 Samples "d" were oven-dried at 110 °C during 24 to 48 hours just before the torrefaction test.

158 **Table 1**. Samples and conditions of the torrefaction experiments

Specimen name	Board thickness (mm)	Initial MC (%)	Heat treatment schedule
HT20d	20	Oven-dry (d)	usual
HT40d	40	Oven-dry (d)	usual

HT40m	40	12 % MC (m)	usual without drying
HT40d-opt	40	Oven-dry (d)	optimized

In total, four specimens were heat-treated. For the study of the effect of the thickness, two of the boards, namely HT20d and HT40d, were oven-dried at 103 °C to remove the residual water before torrefaction with the usual schedule. Then, the third sample, named HT40m and having an initial moisture content of 12 %, was directly heated at 230 °C by omitting the first drying step to study the effect of the residual water on the treatment. The fourth sample, denoted as HT40d-opt, was oven-dried at 103 °C and torrefied with an optimized treatment schedule proposed later in this work.

The overall mass loss (*ML)* due to thermal degradation should be determined as follows:

$$ML = \left[\frac{M_o - M_t}{M_o}\right] 100\% \quad (1)$$

where M_o is the mass at the anhydrous state and M_t is the mass at a time *t* during thermal treatment. However, in this work, the experimental measurements of mass loss do not distinguish between moisture evaporation and wood degradation. Thus, this mass loss is named apparent mass loss (ML_{app}), which is defined by the following equation:

$$ML_{app} = \left[\frac{M_{init} - M_t}{M_{init}}\right] 100\% \quad (2)$$

where M_{init} is the mass of the board in either the moist or dry state, according to the initial conditions at the beginning of the experiment.

2.2.3 Assessing the final density profile and hygroscopicity

The density profiles of the heat-treated boards were scanned by using X-ray attenuation with a Dax5000 from Fagus-GreCon. Samples with dimensions of 50 mm x 50 mm were sawn from the geometric centre of the boards and subsequently dried at 103 °C until reaching constant mass before analysis (Fig. 1b). Besides, the differences in water adsorption capacity between the core and the surface of the torrefied boards (Fig. 1b) were assessed by dynamic vapour sorption (DVS), using a DVS intrinsic apparatus

from Surface Measurement Systems. Samples with 30 to 40 mg mass were subjected to an isothermal cycle at 23 °C of humidification by increasing the relative humidity of the surrounding atmosphere from 0 % up to 90 %, in steps of 15 %. The change in sample mass was followed at regular time intervals (1 point/min). Equilibrium moisture content (EMC %) was considered as established when the change in the sample mass was less than 0.0005 %/min for a given relative humidity level, where this slope is evaluated over a time window of 10 min.

3. Optimization of torrefaction conditions

In this work, a program has been developed to determine tailor-made wood torrefaction conditions to meet the user expectations. The overall mass loss (ML) of the sample is a synthetic indicator of the treatment intensity [24], and it can be used to determine some properties of the torrefied products such as the hygroscopicity, anti-swelling efficiency (ASE), color, grindability and energy content. Just as the final MC is the target of drying, the final ML can be defined as the target of wood torrefaction on the basis of the end user applications. The methodology implemented for the development of the program consists of three complementary parts:

- A torrefaction model computes the ML field over time and the temperature overshoot in the board for a given treatment schedule,
- An objective function is defined to describe the output targets that meet the user expectations,
- A metamodel calls the torrefaction model, starts with a given schedule and modifies it to minimize the objective function.

Each step is presented in detail in the following section.

3.1 Torrefaction model

The 2-D version of the computational model *TransPore,* developed in previous works [22,29–31], was used in this work. This computational model accounts for the thermal decomposition kinetics of the main components of the cell wall (cellulose, hemicelluloses and lignin) via a series of parallel, consecutive or competitive chemical reactions. Enthalpy values are associated with these reactions,

which allows a two-way spatio-temporal coupling between heat and mass transfer and kinetics to be considered: activation of chemical reactions by the local temperature value and evolution of the temperature fields by the cumulative effect of the local heat source due to reactions. In this respect, the temperature computed by *TransPore*, for each control volume of the wood piece, is used to estimate the rate of the chemical reactions and their related heat sources (or sinks) and the production of volatiles. For a better understanding of the intricate two-way coupling between the heat and mass transfer and chemical mechanisms, the formulation of the model at the board scale is summarized in Annex B, and it is presented in more details in the work of Rémond et al. (2010) and Turner et al. (2010) [22,30]. In this work, the initial MC, dimensions and wood density measured on the board samples from our experiments are the input data for the computational model. Additional model parameters come from the literature [22,30]. Finally, the board section is discretized by a set of 41 × 21 control volume, in the radial and tangential directions respectively.

3.2 Module for generating the torrefaction conditions to reach the target ML

A simple module written in Fortran has been developed to generate a wide variety of treatment schedules. This module is integrated in the *TransPore* model, in which the generated schedules are used as boundary conditions of the wood piece, which allows the ML to be computed versus time. In the following, the usual 3-step schedule is generated:

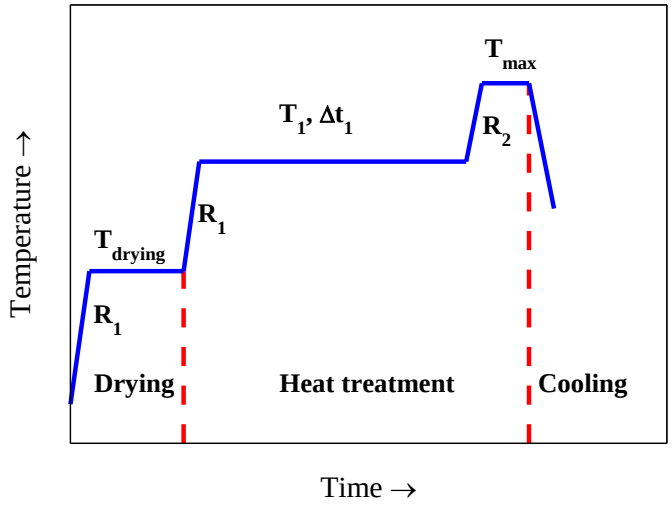

Fig. 3. Example of the torrefaction schedule that can be proposed by the module. This includes a first drying step and two subsequent steps for wood torrefaction.

- Step 1 is a drying stage at a level ranging from 110 °C to 130 °C, maintained until the computed average MC reaches 1%.
- Step 2 is the heat treatment stage itself with two temperature plateaus, the intermediate temperature (T_1) and the maximum torrefaction temperature (T_{max}). The temperature change between plateaus is defined by the heating rate (R_1) and the duration of the intermediate plateau is Δt_1. Step 2 ends as soon as the target ML is reached.
- Step 3 is the cooling stage, which lasts until the reactor temperature drops to 80 °C.

By defining the heating rate (R_1), the parameters of the intermediate plateau (T_1 , Δt_1) and the maximal temperature (T_{max}) as variables of the module, it is already possible to generate a wide variety of torrefaction schedules to reach the target ML (Fig. 3).

3.3 Objective function and variables

An objective function has been built up from three output targets defining the user expectations. The first can be defined by the heterogeneity of the ML field within the wood sample at the end of the treatment, since it is sought to perform a homogeneous treatment of the sample. The second concerns the treatment duration, as good homogeneity should not be sought at the expense of longer durations. The third and last output target intends to limit the exothermic peak which is at the origin of the thermal runaway, hence heterogeneity, observed in industrial ovens. Accordingly, each of the objective variables can be defined as follows:

Firstly, the standard deviation of the ML at the end of the treatment, which is given as a fraction of its mean value $\overline{ML}$,

$$Z_1 = \sigma/\overline{ML} \quad (3)$$

with σ defined as:

$$\sigma = \sqrt{\frac{1}{ncv}\sum_{j=1}^{ncv}(ML(j) - \overline{ML})^2} \quad (4)$$

In the above expression, *ncv* is the total number of control volumes in the board section, and *ML(j)* is the local ML at the control volume *j*.

Secondly, the rate of torrefaction progression establishes the relationship between the duration of the treatment t_{end} and the maximum duration t_{target} accepted by the user:

$$Z_2 = \max\left(0 \;;\; \frac{t_{end} - t_{target}}{t_{target}}\right) \quad (5)$$

Thirdly, the term considering the temperature overshoot, which can be considered as a safety factor to reduce the risk of the thermal runaway, is defined by:

$$Z_3 = \max\left(0 \;;\; \frac{T_{in} - T_{sp}}{T_{sp}}\right) \quad (6)$$

where $T_{in} = \max\left(T(j)_{j=1,ncv}\right)$ during the treatment period, and T_{sp} is the gas temperature around the board surface.

The difficulty remains in finding the right compromise between a short treatment and a homogeneous treatment, while limiting the temperature overshoot. Finally, the global objective function is given as a weighting average of all sub-functions:

$$g = w_1 \cdot Z_1 + w_2 \cdot Z_2 + w_3 \cdot Z_3 \quad (7)$$

where w_i is the weighting factor, such as $w_1 + w_2 + w_3 = 1$, whose value is chosen by the decision maker according to his own constraints.

3.4 Minimization of the objective function

For given torrefaction conditions, the *TransPore* code predicts the values of the objective variables (Z_1, Z_2 , Z_3). A metamodel, developed here in the versatile language Python, calls *TransPore* code by using the F2PY package (*TransPore* being written in the very fast Fortran language) and estimates the value

of the objective function (Eq. 7) [34]. Simulated annealing (SA) has been adopted in the metamodel to minimize this function. We used the dual annealing function included in the SciPy Python Package. A compromise between the quality of the objective function minimum and the number of calls of such function was looked for to limit the time and resource consumption of the SA (Annex A). The program takes 5 minutes for the whole optimization procedure, with two Xenon W cores at 3.5 GHz. The parameters of the SA function were set at the default values [35]: the initial artificial temperature value was 5230, the value of the parameter for visiting distribution was 2.62, the value of the parameter for acceptance distribution was -5, the value of the ratio triggering the restart of the process was 2.10^{-5}, and the local search strategy was deactivated.

Finally, by fixing a target ML, the torrefaction conditions defined by R_1 , T_1, Δt_1, and T_{max} can be tuned by the metamodel to find the best compromise between the three sub-criteria to minimize the objective function.

4. Results and discussion

4.1 Experimental and simulated results

4.2.1 Dynamics of torrefaction treatment

Figures 4a and 4b present the experimental results for the temporal evolution of the core and subsurface temperatures, as well as the ML_{app} for the HT20d and HT40d boards. Both cases were conducted with the usual 3-step schedule (i.e., drying, heating at 230 °C and cooling). It can be observed that at the end of the drying plateau, the core (blue triangle markers) and subsurface (red square markers) temperatures of both boards reach the dry bulb temperature, and the moisture is almost completely removed, as evidenced by the unchanging ML_{app} (grey circle markers). At this point, the remaining MC is almost zero, as shown in Table 2. Subsequently, during heating to the treatment plateau at 230 °C, the temperature in the core exceeds the one at the subsurface of the boards, and both exceed the reactor temperature (black cross markers) until reaching a maximum peak. As is well known, this phenomenon is attributed to the exothermicity of the chemical reactions activated by the rapid increase of the internal temperature of the boards. On the other hand, when the board thickness is doubled, the onset of the

exothermic peak is delayed and its intensity is greater. This is due to a longer time for heat conduction towards the core of the board, and then, when exothermic reactions are activated, the thermal insulation ensured by the sample thickness limits the cooling of the product by the exchange surfaces. Nonetheless, it was also observed that the differences between the core and subsurface temperatures were the same, about 2 °C, for both specimens. This result is unexpected since a greater difference is likely to be observed by doubling the board thickness. This may be attributed to the internal location of the subsurface thermocouple, which was placed 6 mm under the surface of the thickest board, instead of 2 mm as for the thinnest one. Table 2 details the characteristics of the exothermic peaks in terms of the onset time, maximum core and subsurface temperatures, as well as the final ML and ML_{app} of each experiment.

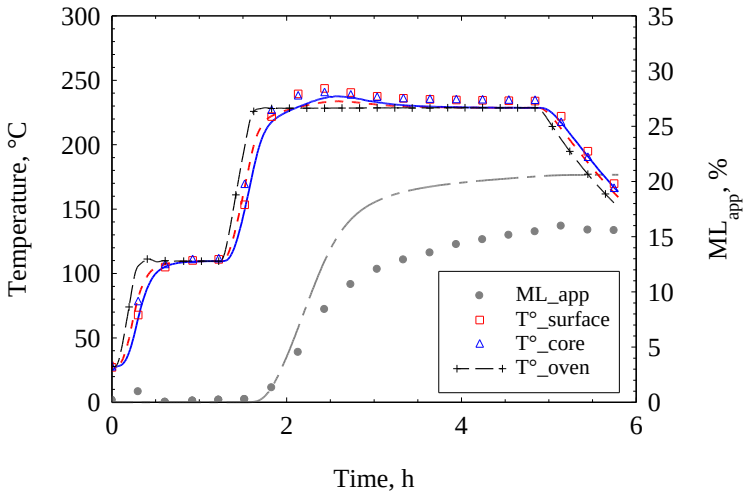

a) 20 mm, dry, HT20d

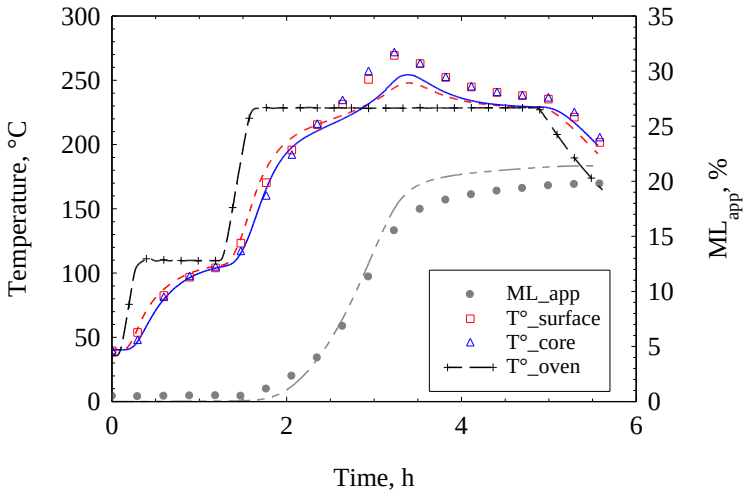

b) 40 mm, dry, HT40d

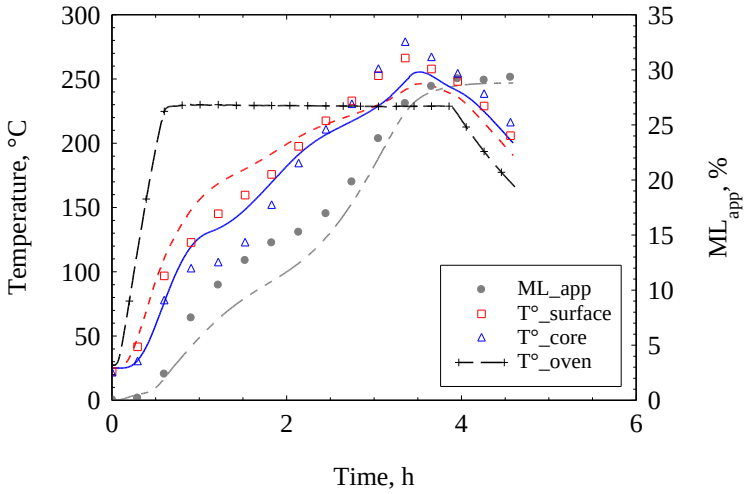

c) 40 mm, moist, HT40m

Fig. 4. Temporal evolution of the ML_{app} (grey circles and dot/dashed curves), core (blue triangles and solid curves) and subsurface (red squares and dashed curves) board temperatures of the samples: (a) HT20d, (b) HT40d and (c) HT40m. Model predictions are represented by the curves and experimental data by the markers.

The subsequent comparison case, shown in Fig. 4c, concerns the evolution of the thermal treatment of the 40 mm thick board with an initial MC at 12 %, which was directly heated at 230 °C for 200 min (without previous drying). Due to the high initial MC, the internal temperature of the board is delayed from the oven temperature, as much of the energy of the system is used to supply the latent heat of

evaporation required to remove the moisture. Thus, because of the massive and sudden water evaporation, the profile of the core temperature exhibits a plateau at 100 °C followed by a sharp increase up to 280 °C after 200 min of heating. Regarding the ML_{app}, as expected, it is higher for the moist board (30 %), but with a true value of ML of the order of 18 %, which is comparable to the dry board (as shown in Table 2), regardless of the differences in the initial MC.

Table 2. Experimental characteristics of the exothermic peaks (onset time, core and subsurface temperatures, T°), and overall mass loss (ML_{app} and ML) of the heat-treated boards.

		Maximum of the exothermic peak				
Specimen name	MC (after drying step)	Time (after drying step)	Core_T°	Subsurface_T°	ML_{app}	ML
	(%)	(min)	(°C)	(°C)	(%)	(%)
HT20d	0	75	239	237	-	16.6
HT40d	0.7	120	271	269	19.8	19.1
HT40m	12.1[a]	215	280	266	30.0	17.8
HT40d-opt	1.5	245	238	238	13.3	11.8

In addition to the results from the three torrefaction experiments presented here, additional experiments (from reference [22] and several unpublished data) using different temperature-levels, duration and heating rates, were tested for model validation. The model predictions for each board are compared to the respective experimental data and plotted as solid lines in Fig. 4. In all the presented cases, the actual temperature in the reactor chamber is used as a boundary condition in the computational model *TransPore*. As can be seen, the model succeeds in predicting with good accuracy the internal board temperatures (core and subsurface) for the very contrasting experimental conditions of sample thickness and initial MC. Regarding the ML_{app} progression, the comparisons are correct for the thickest boards, but it is less good for the HT20d one, since the model seems to overestimate the ML_{app} with a more advanced degradation kinetics. For the three different experimental configurations, the occurrence of the exothermic peak is captured well by the model, but its intensity is under-estimated, notably for the

40 mm thick boards. In the case of the moist board (HT40m), the observed over-predictions on temperature evolution may be related to the local pressure at the internal position of the probes, which seems to be at atmospheric pressure with a plateau at 100°C despite the intense evaporation of the bound water, while the model predicts a local overpressure of about 2.5 bar. A possible cause would be a leakage around the tight connector that links the board to the probe.

4.2.2 Heterogeneity of treatment intensity across the sample thickness

The intensity of the different heat treatments was then experimentally compared by measuring the changes in the density profile and water sorption capacity of the beech boards before and after torrefaction. The ability of the Grecon X-ray beam to detect density changes after heat treatment was first verified using a series of homogeneously heat-treated thin beech specimens with different mass losses. It was found that the Grecon analyzer is capable of accurately measuring small changes in mean density, even as little as 10 kg/m^3. Figure 5a compares the density profile of the HT40d specimen with the untreated reference, both of which have the same pattern of annual growth rings. Since the X-ray beam scans were performed in the radial direction, i.e., the X-ray passes through the sample in the tangential direction, the growth rings were highlighted, and the alternation between earlywood (EW, lower density) and latewood (LW, higher density) was distinguished by the lowest and the highest density values of each peak, respectively.

As can be seen, the case corresponding to the heat-treated specimen displays more pronounced and narrower peaks that are positioned at lower density values than the untreated reference, due to the degradation and shrinking of the cell wall during torrefaction. At the same time, the density reduction seems to be greater in earlywood than in latewood, as evidenced by the decrease of the respective peaks, notably those placed at the half-length of the board, where the highest temperature overshoot was recorded. These results are consistent with studies performed on different wood species [36,37]. The higher susceptibility of earlywood to thermal degradation can be attributed to a lower proportion of the cellulose content, since its S2 layer is thinner, thus increasing the proportion of the more thermally sensitive components, namely hemicelluloses and lignin, to heat degradation, while cellulose remains

stable at the recorded temperatures. In addition, greater shrinkage of LW compared to EW due to cell wall component degradations could also explain this observation, since shrinkage increases density, hence counterbalancing the mass loss per unit volume.

These trends obviously cannot be captured by the model, which considers a homogeneous density in the board at the initial state (here 698 kg m^{-3} for the untreated 40 mm thick board). Fig. 5b shows that the model simulates a parabolic density profile at the end of the treatment, with a slightly lower density at the core than at the surface.

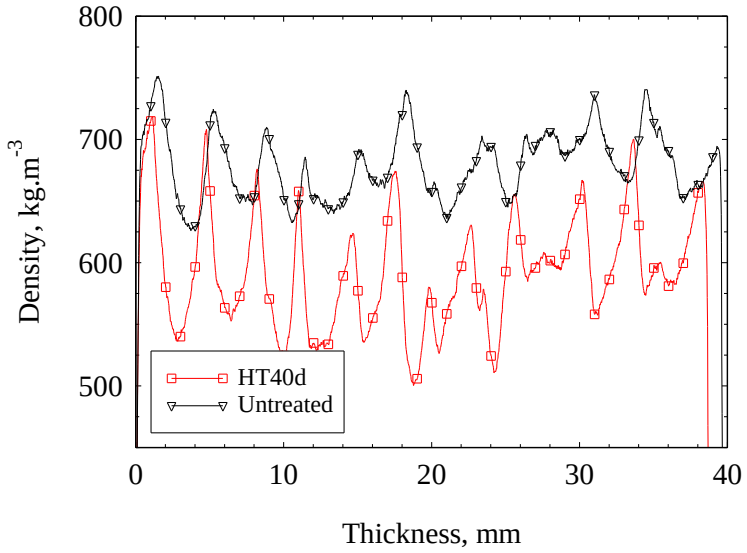

a) experiments

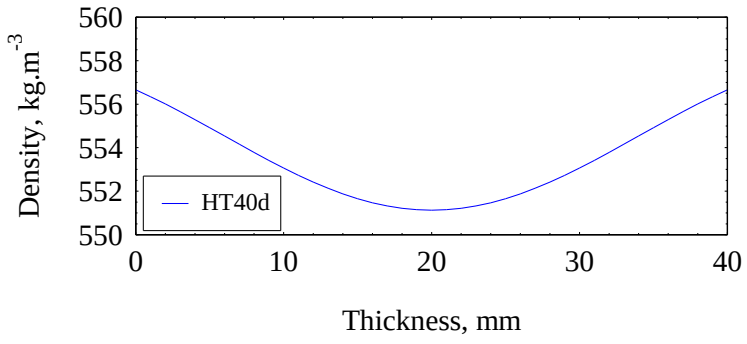

b) model

Fig. 5. Density profile across the thickness (radial direction on the RT plan) of the HT40d board (a) measured before and after heat treatment and (b) predicted by the model after treatment.

For all other specimens, the changes in their density profile are not presented here because the pattern of the annual rings was very different from the untreated reference, making it difficult to draw conclusions about the extent of the local degradation. The mean density of all heat-treated specimens is shown in Table 3.

Table 3. Mean density of heat treated and untreated beech wood measured by tomography. Two specimens were analysed at each time.

Specimen	Mean density ($kg\ m^{-3}$)	Standard deviation ($kg\ m^{-3}$)
Untreated, 20 mm	671.8	26.1
HT20d	558.6	54.1
Untreated, 40 mm	698.5	34.4
HT40d	580.2	8.7
HT40m	575.0	3.0
HT40d_opt	604.1	7.0

Fig. 6 shows the changes in hygroscopicity after the heat treatment, as well as the differences in the adsorption isotherms between the core (C, solid marks) and the outer surface layer (S, empty marks) of the dry boards, namely HT20d and HT40d. In both cases, the EMC of the untreated beech decreases over the analyzed range of relative humidity (i.e., 0 % to 90 %). It is well known that heat treatment reduces the sorption isotherms. The measurement presented here perfectly confirms this: first, a slight reduction at the surface, in agreement with the density and temperature evolution; second, a larger reduction at the core due to the overshoot in temperature, which triggers kinetics; third, an effect of the thickness, which exacerbates the overshoot due to a thicker insulation.

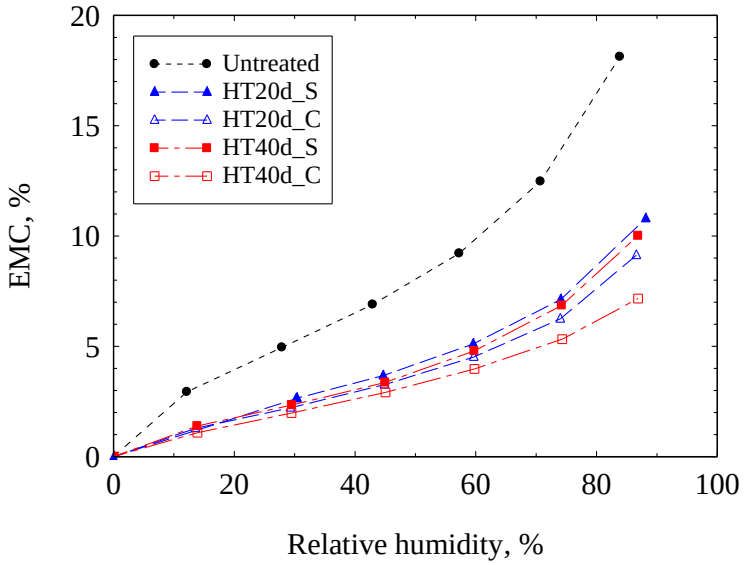

a) isotherms

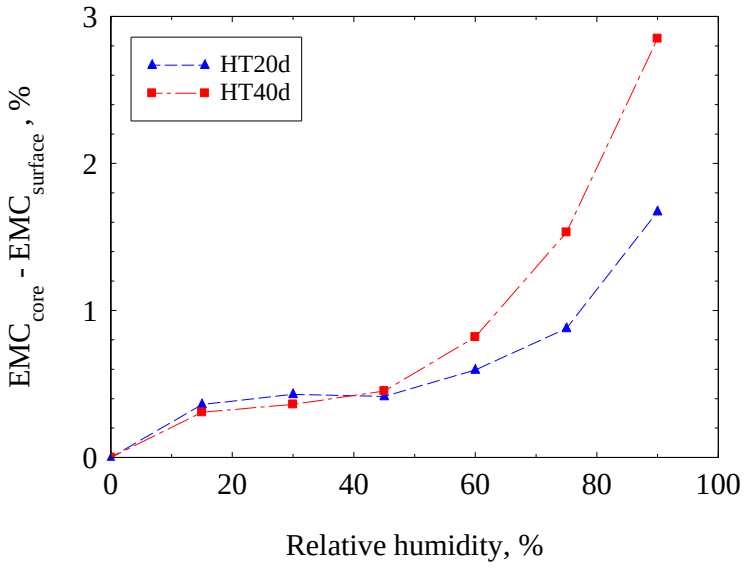

b) core-surface isotherms differences

382 **Fig. 6**. Effect of treatment on water adsorption capacity: untreated (black dots) and torrefied samples
383 from core (C, solid dots) and outer surface layer (S, empty dots) of the boards of different thicknesses.
384 a) Sorption isotherms and b) Isotherm differences between core and surface.

385

4.2 Numerical analysis of the time–temperature couples for a single step treatment

From the above, it becomes evident that the intensity of the heat treatment is very sensitive to the wood properties and initial conditioning, hence the need to adapt the treatment schedule to each particular case. To further investigate the effect of board thickness on the time–temperature couple, when a single temperature step treatment is applied, a series of simulations were carried out for varying the board thickness, namely 10 mm, 18 mm, 34 mm and 54 mm (in the radial (R) direction of the wood), for a 150 mm wide board (in the tangential (T) direction) and for a target ML equal to 15 %. At the beginning of the treatment, the boards are assumed to be anhydrous and at a temperature of 100 °C. Subsequently, these are subjected to a single-step schedule at constant temperature, for an undefined period of time until the desired ML is reached.

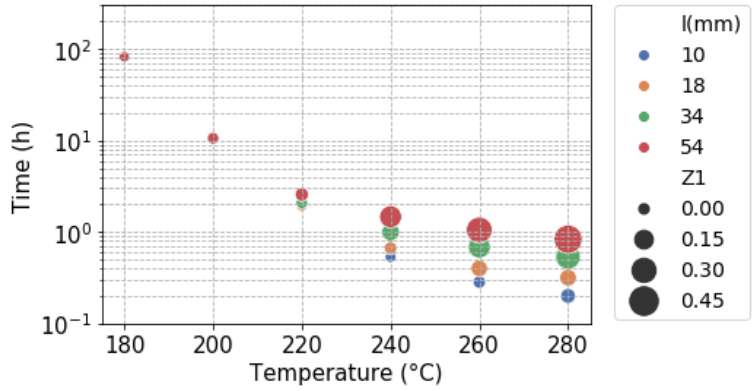

a) Z1

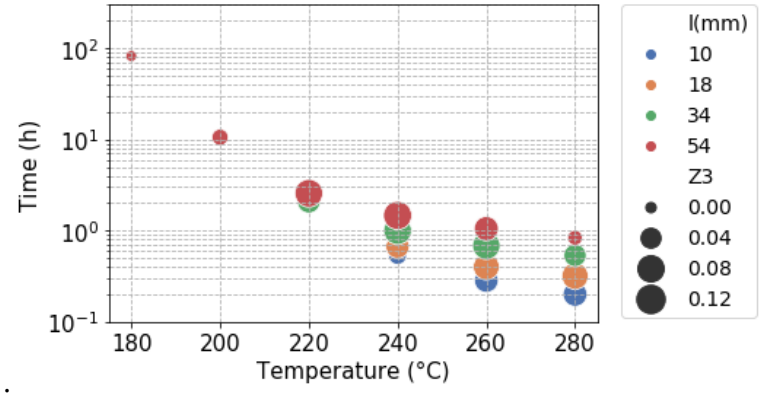

.

b) Z3

Fig. 7. Comparison of the time–temperature couples and their respective values of: (a) Z1 and (b) Z3, for a single-step torrefaction program for boards of different thickness (l) with a target ML of 15 %. The values of the objective variable are represented by the diameter of the circles.

Fig. 7 shows the time–temperature couples proposed to reach a target ML of 15 % for each thickness (*l*, color of the circles), as well as the values (diameter of the circles) of two objective variables, Z_1 (Fig. 7a) and Z_3 (Fig. 7b). Remember that Z1 (Eq. 3) estimates the relative ML heterogeneity at the end of the thermal treatment and Z_3 (Eq. 6) quantifies the temperature overshoot. These graphs highlight the effect of thermal activation of the exothermic reactions: a clear time–temperature equivalence is revealed by the time–temperature couples. For instance, for a 10 mm thick board, the treatment duration is 82 h at 180 °C compared to 0.2 h at 280 °C. In fact, at low temperature levels (e.g., below 200 °C), the duration of the heat treatment is independent of the board thickness: the time required to reach a ML of 15 % is much longer than the characteristic time of heat diffusion in the board thickness. Whatever the thickness, the temperature remains quasi-uniform and the overshoot is low (see Fig. 7a). In contrast, as the temperature rises above 220 °C, the residence time is of the same order of magnitude as the diffusion time constant of the wood piece. Whether during heating or in the exothermic phase, step temperature profiles are established during the process. Consequently, the treatment time and its heterogeneity depend on the board thickness. This is confirmed by the relative heterogeneity at the end of torrefaction, quantified by Z1 (Fig. 7a).

This criterion increases with temperature and, in a more intensive manner, with the sample thickness. Note that the area where the temperature is maximum does not correspond necessarily to greater degradation rates since, as mentioned above, the degradation profile is a result of the history of the temperature profile in time (Fig. 8).

Finally, Fig. 7b represents the evolution of the temperature overshoot or Z_3 as a function of temperature, where an inflection point around 220 °C to 240 °C is revealed for the thickest samples. In fact, given that the duration of the treatment is similar to or less than the diffusion constant time, the temperature increase at the core of the board is not high enough to activate the exothermic reactions. In this case, the

temperature overshoot is attenuated and the treatment is larger at the surface than in the core of the board.

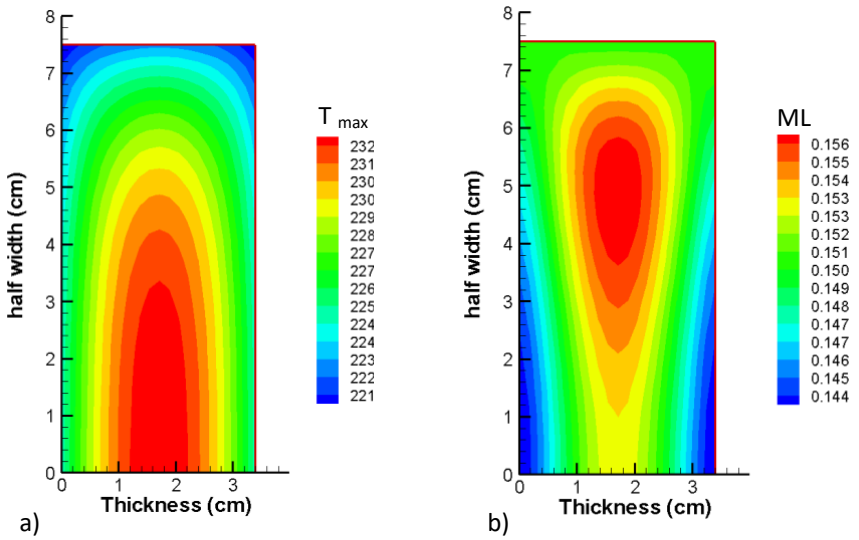

Fig. 8. (a) Field of the maximum temperature T_{max} reached throughout the process for each location at 220 °C of a 35 mm thick board; (b) degradation field at the end of the treatment in the radial (x-axis) – tangential (y-axis) plane. The y-axis represents the distance from the half-width of the board.

It is seen here that the impact of the torrefaction conditions on the objective variables is quite subtle. The empirical approach to find the adapted sequence of the temperature levels–duration couples is a very laborious task. Accordingly, the optimisation procedure proposed in this work makes sense to find the most suitable torrefaction conditions to meet the user expectation.

4.3 Case study: experimental validation of 4-step torrefaction program proposed by the model

In the torrefaction experiments presented above, it seems difficult to limit the magnitude of the exothermic peak with the usual 3-step program. In fact, a gradual temperature increase or the addition of an intermediate step in the treatment program causes the chemical reactions to proceed at a reasonable rate while limiting the thermal runaway. In an attempt to reduce these undesirable effects, which is such a difficult task, the optimization algorithm of the objective function was employed. More specifically, in this case study, the process was optimized only in terms of the duration of the treatment (Z_2) and reduction of the temperature overshoot (Z_3) by fixing, in Eq. (7), w_1=0, w_2=0.3 and w_3=0.7. This choice

was made because these two variables can be easily evaluated during the process. In this sense, the optimization variables considered according to the 4-step treatment schedule, illustrated in Fig. 3, were T_1 and Δt_1, while the values of the other variables were fixed as: T_{max}=230 °C; T_{drying}=110 °C; R_1= 5 °C min^{-1}; t_{target} =5 h (without the cooling step); for a target ML equal to 15 %. T_1 can be tuned by the SA in the metamodel between 190 °C and 210 °C and Δt_1 between 100 min and 240 min.

It is interesting to note that the optimal treatment schedule given by the SA method implemented in this work chooses the maximum temperature allowed for T1 to limit both the residence time at 230 °C and the duration of the treatment. Moreover, it uses the cooling phase to control the exothermic peak.

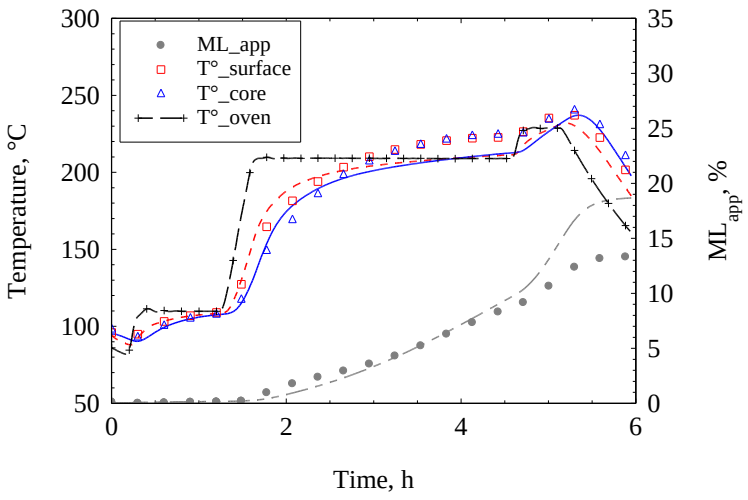

Fig. 9. Comparison between model predictions and experimental data of heat-treatment progression of a beech board (40 mm thick, anhydrous) torrefied with the 4-step schedule proposed by the model. Model predictions are represented by the curves and experimental data by the markers.

Subsequently, the proposed schedule was performed experimentally on a 40 mm thick dry board named as HT40d-opt. The comparison of the experimental course of the torrefaction with the predictions of the model is shown in Fig. 9. The experimental results in terms of the characteristics of the exothermic peak and the final ML_{app}, as well as the mean density measured by X-ray, are shown in Tables 2 and 3, respectively. The temperature overshoot at the core is now 8 °C on this optimized schedule, as against 41 °C for the twin board on the first schedule (compare HT40d-opt vs. HT40d, Table 2) for an identical

treatment duration (4 h). The overall ML reached experimentally is 11.8 % (Table 3), which is lower than the fixed target of 15 %.

From the above, the model proved its ability to propose optimized schedules able to fulfill the desired criteria, but also to correctly predict the experimental behavior for this schedule with 2 treatment plateaus, more demanding than the initial experiments.

5. Conclusions

An optimization program proposing tailor-made torrefaction schedules (temperature levels–duration) has been derived to control the torrefaction process of wood. This opens up the possibility of controlling the ultimate product qualities according to the user expectations. In this regard, the main outcomes of this work can be summarised as follows:

- A torrefaction device was developed to thermally treat instrumented wood sample under contrasting conditions,
- Parameters such as sample thickness and initial moisture content influence the temperature overshoot and overall mass loss,
- The water sorption isotherms are accurate for evaluating the heterogeneity of this treatment,
- A mechanistic model was used to successfully simulate these experiments,
- The use of an optimization procedure allows the treatment schedule to be adapted while mitigating the temperature overshoot,
- The predictive potential of the model has been experimentally validated with this optimized schedule.

Discrepancies were evidenced in comparisons between measurements and simulations of the intensity of the exothermic peak and the magnitude of the mass loss. An adjustment of some parameters of the heat treatment model or the implementation of the new model proposed by [38] appears a promising development of this work. Furthermore, this optimization approach, validated at the scale of one board,

could be developed in a double-scale modelling of a board stack [23] or a packed bed of chips to optimize the schedules and avoid the thermal runaway in the industrial heat treatment process.

6. Funding

This research did not receive any specific grant from funding agencies in the public, commercial, or not-for-profit sectors.

7. References

[1] Lv P, Almeida G, Perré P. TGA-FTIR Analysis of torrefaction of lignocellulosic components (cellulose, xylan, lignin) in isothermal conditions over a wide range of time durations. BioResources 2015;10:4239–51.

[2] Qu T, Guo W, Shen L, Xiao J, Zhao K. Experimental study of biomass pyrolysis based on three major components: hemicellulose, cellulose, and lignin. Ind Eng Chem Res 2011;50:10424–33. https://doi.org/10.1021/ie1025453.

[3] Rousset P, Lapierre C, Pollet B, Quirino W, Perre P. Effect of severe thermal treatment on spruce and beech wood lignins. Ann For Sci 2009;66:110–110. https://doi.org/10.1051/forest/2008078.

[4] Shen DK, Gu S, Luo KH, Wang SR, Fang MX. The pyrolytic degradation of wood-derived lignin from pulping process. Bioresource Technology 2010;101:6136–46. https://doi.org/10.1016/j.biortech.2010.02.078.

[5] Shen DK, Gu S. The mechanism for thermal decomposition of cellulose and its main products. Bioresource Technology 2009;100:6496–504. https://doi.org/10.1016/j.biortech.2009.06.095.

[6] Wu Y, Zhao Z, Li H, He F. Low temperature pyrolysis characteristics of major components of biomass. Journal of Fuel Chemistry and Technology 2009;37:427–32. https://doi.org/10.1016/S1872-5813(10)60002-3.

[7] Yang H, Yan R, Chen H, Lee DH, Zheng C. Characteristics of hemicellulose, cellulose and lignin pyrolysis. Fuel 2007;86:1781–8. https://doi.org/10.1016/j.fuel.2006.12.013.

[8] Bourgois J, Guyonnet R. Characterization and analysis of torrefied wood. Wood SciTechnol 1988;22:143–55. https://doi.org/10.1007/BF00355850.

[9] Stamm AJ, Burr HK, Kline AA. Staybwood—Heat-stabilized wood. Ind Eng Chem 1946;38:630–4. https://doi.org/10.1021/ie50438a027.

[10] Viitaniemi P. Decay-resistant wood created in a heating process - a heat-treatment process of wood development by VTT building Technology yields timber products with enhanced properties. Industrial Horizons 1997:22–3.

[11] Almeida G, Brito JO, Perré P. Alterations in energy properties of eucalyptus wood and bark subjected to torrefaction: The potential of mass loss as a synthetic indicator. Bioresource Technology 2010;101:9778–84. https://doi.org/10.1016/j.biortech.2010.07.026.

[12] Ong HC, Yu KL, Chen W-H, Pillejera MK, Bi X, Tran K-Q, et al. Variation of lignocellulosic biomass structure from torrefaction: A critical review. Renewable and Sustainable Energy Reviews 2021;152:111698. https://doi.org/10.1016/j.rser.2021.111698.

[13] Pierre F, Almeida G, Colin J, Perré P. Reduction of biomass resilience by torrefaction: apparent stiffness during failure (ASF) and specific failure energy (SFE) assessed by a custom impact device. Holzforschung 2017;71:863–72. https://doi.org/10.1515/hf-2016-0191.

[14] Kota KB, Shenbagaraj S, Sharma PK, Sharma AK, Ghodke PK, Chen W-H. Biomass torrefaction: An overview of process and technology assessment based on global readiness level. Fuel 2022;324:124663.

[15] Kumar L, Koukoulas AA, Mani S, Satyavolu J. Integrating torrefaction in the wood pellet industry: A critical review. Energy Fuels 2017;31:37–54. https://doi.org/10.1021/acs.energyfuels.6b02803.

[16] Zulfiqar M, Moghtaderi B, Wall TF. Flow properties of biomass and coal blends. Fuel Processing Technology 2006;87:281–8.

[17] Thrän D, Witt J, Schaubach K, Kiel J, Carbo M, Maier J, et al. Moving torrefaction towards market introduction – Technical improvements and economic-environmental assessment along the overall torrefaction supply chain through the SECTOR project. Biomass and Bioenergy 2016;89:184–200. https://doi.org/10.1016/j.biombioe.2016.03.004.

[18] Girods P, Dufour A, Rogaume Y, Rogaume C, Zoulalian A. Thermal removal of nitrogen species from wood waste containing urea formaldehyde and melamine formaldehyde resins. Journal of Hazardous Materials 2008;159:210–21. https://doi.org/10.1016/j.jhazmat.2008.02.003.

[19] Besserer A, Troilo S, Girods P, Rogaume Y, Brosse N. Cascading recycling of wood waste: A review. Polymers 2021;13:1752. https://doi.org/10.3390/polym13111752.

[20] Branca C, Di Blasi C, Galgano A. Chemical characterization of volatile products of biomass pyrolysis under significant reaction-induced overheating. Journal of Analytical and Applied Pyrolysis 2016;119:8–17. https://doi.org/10.1016/j.jaap.2016.04.004.

[21] Di Blasi C, Branca C, Galgano A. On the experimental evidence of exothermicity in wood and biomass pyrolysis. Energy Technol 2017;5:19–29. https://doi.org/10.1002/ente.201600091.

[22] Turner I, Rousset P, Rémond R, Perré P. An experimental and theoretical investigation of the thermal treatment of wood (Fagus sylvatica L.) in the range 200–260°C. International Journal of Heat and Mass Transfer 2010;53:715–25. https://doi.org/10.1016/j.ijheatmasstransfer.2009.10.020.

[23] Perré P, Rémond R, Turner I. A comprehensive dual-scale wood torrefaction model: Application to the analysis of thermal run-away in industrial heat treatment processes. International Journal of Heat and Mass Transfer 2013;64:838–49. https://doi.org/10.1016/j.ijheatmasstransfer.2013.03.066.

[24] Almeida G, Brito JO, Perré P. Changes in wood-water relationship due to heat treatment assessed on micro-samples of three Eucalyptus species. Holzforschung 2009;63. https://doi.org/10.1515/HF.2009.026.

[25] Brischke C, Welzbacher CR, Brandt K, Rapp AO. Quality control of thermally modified timber: Interrelationship between heat treatment intensities and CIE L*a*b* color data on homogenized wood samples. Holzforschung 2007;61:19–22. https://doi.org/10.1515/HF.2007.004.

[26] Candelier K, Thevenon M-F, Petrissans A, Dumarcay S, Gerardin P, Petrissans M. Control of wood thermal treatment and its effects on decay resistance: a review. Annals of Forest Science 2016;73:571–83. https://doi.org/10.1007/s13595-016-0541-x.

[27] Candelier K, Hannouz S, Elaieb M, Collet R, Dumarçay S, Pétrissans A, et al. Utilization of temperature kinetics as a method to predict treatment intensity and corresponding treated wood quality: Durability and mechanical properties of thermally modified wood. Maderas, Cienc Tecnol 2015:0–0. https://doi.org/10.4067/S0718-221X2015005000024.

[28] Candelier K, Dumarçay S, Pétrissans A, Gérardin P, Pétrissans M. Comparison of mechanical properties of heat treated beech wood cured under nitrogen or vacuum. Polymer Degradation and Stability 2013;98:1762–5. https://doi.org/10.1016/j.polymdegradstab.2013.05.026.

[29] Perré P, Turner IW. A 3-D version of TransPore: a comprehensive heat and mass transfer computational model for simulating the drying of porous media. International Journal of Heat and Mass Transfer 1999;42:4501–21. https://doi.org/10.1016/S0017-9310(99)00098-8.

[30] Rémond R, Turner I, Perré P. Modeling the drying and heat treatment of lignocellulosic biomass: 2D effects due to the product anisotropy. Drying Technology 2010;28:1013–22. https://doi.org/10.1080/07373937.2010.497093.

[31] Rousset P. Choix et validation expérimentale d'un modèle de pyrolyse pour le bois traité par haute température : de la micro-particule au bois massif. Theses. Paris, ENGREF, 2004.

[32] Colin J. Séchage en continu du bois énergie comme moyen de préconditionnement en vue de sa conservation thermochimique : approches expérimentale et numérique. Theses. AgroParisTech, 2011.

[33] Challansonnex A, Casalinho J, Perré P. Non-Fickian diffusion in biosourced materials: Experimental determination of the memory function using minute samples. Construction and Building Materials 2019;224:560–71. https://doi.org/10.1016/j.conbuildmat.2019.07.013.

[34] Peterson P. F2PY: a tool for connecting Fortran and Python programs. International Journal of Computational Science and Engineering 2009;4:296–305. https://doi.org/10.1504/IJCSE.2009.029165.

[35] Xiang Y, Gubian S, Suomela B, Hoeng J. Generalized simulated annealing for global optimization: the GenSA package. R J 2013;5:13.

[36] Hamada J, Pétrissans A, Ruelle J, Mothe F, Colin F, Pétrissans M, et al. Thermal stability of Abies alba wood according to its radial position and forest management. Eur J Wood Prod 2018;76:1669–76. https://doi.org/10.1007/s00107-018-1353-5.

[37] Shchupakivskyy R, Clauder L, Linke N, Pfriem A. Application of high-frequency densitometry to detect changes in early- and latewood density of oak (Quercus robur L.) due to thermal modification. Eur J Wood Prod 2014;72:5–10. https://doi.org/10.1007/s00107-013-0744-x.

[38] Perré P, Tian Y, Lu P, Malinowska B, Bekri JE, Colin J. A robust and frugal model of biomass pyrolysis in the range 100–800 °C: Inverse analysis of DAEM parameters, validation on static tests and determination of heats of reaction. Fuel 2021;288:119692. https://doi.org/10.1016/j.fuel.2020.119692.

[39] Whitaker S. Simultaneous Heat, Mass, and Momentum Transfer in Porous Media: A Theory of Drying. In: Hartnett JP, Irvine TF, editors. Advances in Heat Transfer, vol. 13, Elsevier; 1977, p. 119–203. https://doi.org/10.1016/S0065-2717(08)70223-5.

Annex A: SA results by the numbers of calls

Figure A.1 shows the results of the SA with different numbers of calls of the objective function, which is implemented in the code in the "maxfun" parameter. In this paper, this parameter was set to 100 for the search for the optimised thermal treatment schedule.

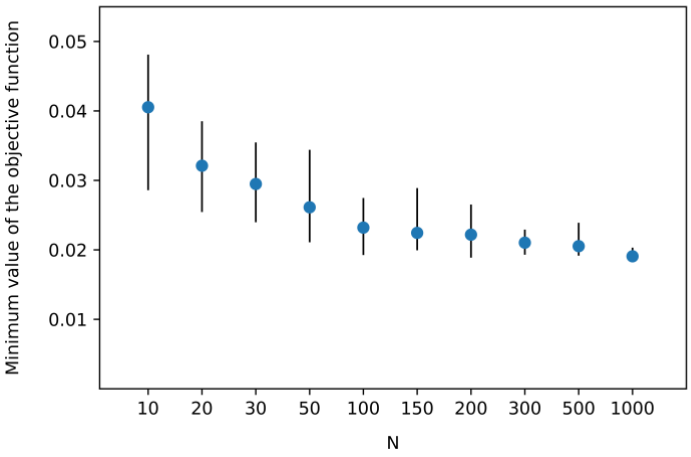

608

609 **Fig. A.1.** Minimum value of the objective function called by the algorithm: N represents the number of
610 calls of the objective function. The blue marker is the mean value of 10 numerical tests, and the error
611 bars represent the difference between the minimum and maximum of the objective function.

612 **Annex B: Formulation of the torrefaction model. Summarized from** [22]

613 The total behaviour of wood is obtained from the evolution of its principal components:

614 $$Wood = \%\ cellulose + \%\ lignin + \%\ hemicellulose$$

615 The following system of differential equations is used for the degradation of the wood components (the
616 kinetics parameters are depicted in table A1).

617 - *Hemicellulose*

618
$$\begin{aligned} &\frac{d\rho_H}{dt} = -k_1 \cdot \rho_H \ , && \frac{d\rho_{G_1}}{dt} = 0.43 \cdot k_1 \cdot \rho_H \ , \\ &\frac{d\rho_{S_1}}{dt} = -k_2 \cdot \rho_{S_1} + 0.57 \cdot k_1 \cdot \rho_H \ , && \frac{d\rho_{G_2}}{dt} = 0.56 \cdot k_2 \cdot \rho_{S_1} \ , \\ &\frac{d\rho_{S_2}}{dt} = 0.44 \cdot k_2 \cdot \rho_{S_1} \ , \end{aligned} \qquad (1)$$

619 where ρ_H represents the mass of hemicellulose; k_1 and k_2 the reaction rates and ρ_{S_i}, ρ_{G_i} the
620 masses of the coal or tar and volatile matters produced during reaction $i = 1,2$.

621 - *Cellulose*

622
$$\frac{d\rho_C}{dt} = -(k_3 + k_4)\rho_C \ , \qquad \frac{d\rho_{G_4}}{dt} = k_4 \rho_C \ , \qquad (2)$$

where ρ_C is the mass of cellulose and k_3 and k_4 are the reaction rates for cellulose.

- Lignin

$$\frac{d\rho_L}{dt} = -k_5\rho_L \ , \qquad \frac{d\rho_{G_5}}{dt} = k_5\rho_L \ , \tag{3}$$

where ρ_L is the mass of lignin and k_5 is the reaction rate for lignin. In the above equations we model the reaction rates according to the Arrenhius Law $k_i = A_i \exp\left(\frac{-E_i}{RT}\right)$.

Table A1. *Parameters used for the wood pyrolysis model. H, C, L designate respectively hemicellulose, cellulose, lignin; G_i and S_i designate the products from the reaction i respectively in the gaseous phase and in the solid phase.*

Component	Models	Kinetics parameters
Hemicelluloses	H $\xrightarrow{1}$ 0,43 G_1 + 0.57 S_1 H $\xrightarrow{2}$ 0,56 G_2 + 0.44 S_2	E_1 = 193 kJ/mol A_1= 7, 94.10 ^{16} s^{-1} E_2 = 95 kJ/mol A_2 = 5,01.10^6 s^{-1}
Cellulose	C $\xrightarrow{3}$ S_3 C $\xrightarrow{4}$ G_4	E_3 = 147 kJ/mol A_3 = 2.51.10 ^{9} s^{-1} E_4 = 238 kJ/mol A_4= 1.25.10 ^{18} s^{-1}
Lignin	L $\xrightarrow{5}$ S_5 + G_5	E_5 = 124.3 kJ/mol A_5 = 2.77.10 ^{7} s^{-1}

The macroscopic conservation equations governing heat and mass transfer phenomena in porous media during drying [29], [39] were extended in [22] to account for the effects of chemical reactions (component degradation, heat source, heat sink and volatiles production). The control volume (CV) method is implemented to discretize the conservation laws. Thereafter, an efficient inexact Newton method is used to solve the complicated nonlinear system that describes the drying and heat treatment processes.